

GABAergic Projections from the Medial Septum Selectively Inhibit Interneurons in the Medial Entorhinal Cortex

Alfredo Gonzalez-Sulser,¹ Daniel Parthier,¹ Antonio Candela,¹ Christina McClure,¹ Hugh Pastoll,¹ Derek Garden,¹ Gülşen Sürmeli,¹ and Matthew F. Nolan¹

Centre for Integrative Physiology, University of Edinburgh, Hugh Robson Building, Edinburgh EH8 9XD, United Kingdom

The medial septum (MS) is required for theta rhythmic oscillations and grid cell firing in the medial entorhinal cortex (MEC). While GABAergic, glutamatergic, and cholinergic neurons project from the MS to the MEC, their synaptic targets are unknown. To investigate whether MS neurons innervate specific layers and cell types in the MEC, we expressed channelrhodopsin-2 in mouse MS neurons and used patch-clamp recording in brain slices to determine the response to light activation of identified cells in the MEC. Following activation of MS axons, we observed fast monosynaptic GABAergic IPSPs in the majority (>60%) of fast-spiking (FS) and low-threshold-spiking (LTS) interneurons in all layers of the MEC, but in only 1.5% of nonstellate principal cells (NSPCs) and in no stellate cells. We also observed fast glutamatergic responses to MS activation in a minority (<5%) of NSPCs, FS, and LTS interneurons. During stimulation of MS inputs at theta frequency (10 Hz), the amplitude of GABAergic IPSPs was maintained, and spike output from LTS and FS interneurons was entrained at low (25–60 Hz) and high (60–180 Hz) gamma frequencies, respectively. By demonstrating cell type-specific targeting of the GABAergic projection from the MS to the MEC, our results support the idea that the MS controls theta frequency activity in the MEC through coordination of inhibitory circuits.

Key words: gamma; interneuron; lamina organization; medial entorhinal cortex; medial septum; theta

Introduction

Spatial firing by neurons in the medial entorhinal cortex (MEC) is associated with theta frequency (4–11 Hz) oscillations in network activity (Mitchell and Ranck, 1980; Chrobak and Buzsáki, 1998; Colgin et al., 2009; Newman et al., 2013). Theta modulation of the MEC has lamina- and cell type-specific organization. For example, grid cells in layer II fire action potentials that precess relative to the theta rhythm, whereas grid cells in layer III fire action potentials at a fixed phase relative to the theta rhythm (Hafting et al., 2008; Mizuseki et al., 2009). The phase and power of theta and associated nested gamma oscillations also vary between the lamina of the MEC (Chrobak and Buzsáki, 1998; Mizuseki et al., 2009; Quilichini et al., 2010). The medial septum (MS), which contains interacting populations of glutamatergic,

GABAergic, and cholinergic projection neurons, is critical to theta activity and grid firing. Inactivation of the MS reversibly abolishes theta frequency oscillations and grid firing patterns (Mitchell et al., 1982; Brandon et al., 2011; Koenig et al., 2011). However, while anatomical studies establish direct projections from the MS to the MEC (Meibach and Siegel, 1977; Mitchell et al., 1982), we know very little about the synaptic targets of these projections or their cellular mechanisms of action.

To address this, we investigate synaptic responses of MEC neurons in brain slices following optical activation of axons from MS neurons expressing channelrhodopsin 2 (ChR2). We find that a high proportion of GABAergic interneurons across all layers of the MEC receive monosynaptic GABAergic inputs from the MS. Activation of GABAergic input from the MS at theta frequencies entrains low-frequency (25–60 Hz) and high-frequency (60–180 Hz) action potential firing by low-threshold-spiking (LTS) and fast-spiking (FS) interneurons respectively.

Materials and Methods

Surgical procedure. Experiments used C57BL/6J OlaHsd (RRID:IMSR-JAX:000664) 8- to 10-week-old male mice, were approved by the University of Edinburgh animal welfare committee, and were performed under a UK Home Office project license. Animals were anesthetized with isoflurane and mounted in a stereotaxic frame (David Kopf Instruments). Adeno-associated virus (AAV) expressing either ChR2 conjugated with Venus fluorescent protein (pACAGW-ChR2-Venus-AAV serotype 2/1; generated by Vector Biolabs, from Plasmid 20071, AddGene) or ChR2 conjugated with mCherry [AAV-hSyn-hChR2(H134R)-mCherry serotype 2, University of North Carolina Vector Core, Chapel Hill, NC] was injected through a craniotomy 0.3 mm lateral to the midline and 0.6 mm caudal to bregma. Two injections of 400 nl were made at

Received April 21, 2014; revised Oct. 15, 2014; accepted Oct. 18, 2014.

Author contributions: A.G.-S., H.P., D.G., and M.F.N. designed research; A.G.-S., D.P., A.C., C.M., H.P., D.G., and G.S. performed research; C.M. and G.S. contributed unpublished reagents/analytic tools; A.G.-S., D.P., H.P., D.G., and G.S. analyzed data; A.G.-S. and M.F.N. wrote the paper.

This work was supported by the Biotechnology and Biological Sciences Research Council (BBSRC Grants BB/L010496/1 and BB/H020284/1 to M.F.N.), a Marie-Curie International Incoming Post-Doctoral Fellowship (629586 to A.G.-S.), and a Sir Henry Wellcome Postdoctoral Fellowship (098915/Z/12/z to G.S.). We thank the IMPACT facility at the University of Edinburgh for imaging resources.

The authors declare no competing financial interests.

This article is freely available online through the *JNeurosci* Author Open Choice option.

Correspondence should be addressed to Matthew F. Nolan, Centre for Integrative Physiology, Hugh Robson Building, 15 George Square, Edinburgh EH8 9XD, UK. E-mail: mattnolan@ed.ac.uk.

DOI:10.1523/JNEUROSCI.1612-14.2014

Copyright © 2014 Gonzalez-Sulser et al.

This is an Open Access article distributed under the terms of the Creative Commons Attribution License (<http://creativecommons.org/licenses/by/3.0/>), which permits unrestricted use, distribution and reproduction in any medium provided that the original work is properly attributed.

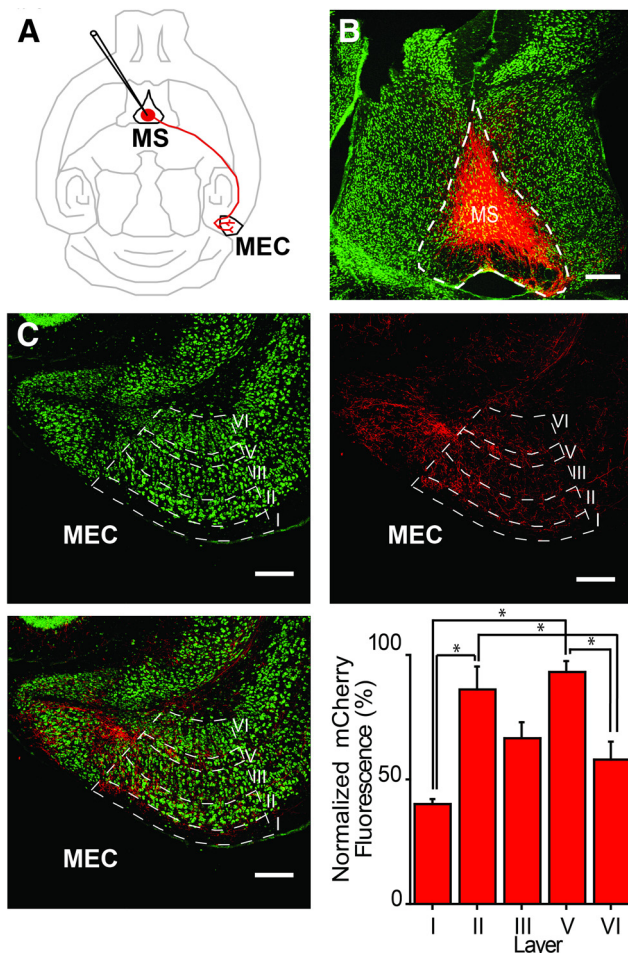


Figure 1. Labeling of axonal projections from MS to MEC. **A**, Diagram illustrating AAV injection site in the MS and labeled axonal projections (red) to the MEC. **B**, ChR2-mCherry-expressing cells (red) in a horizontal section containing the MS and also labeled with NeuroTrace (green). **C**, Horizontal section of the MEC, with cell bodies labeled with NeuroTrace (top left), MS axons expressing ChR2-mCherry (top right), and merged image (bottom left). Normalized mCherry fluorescence quantification reveals differences between layers (bottom right; * $p < 0.05$, Tukey's test). Scale bars, 200 μm .

3.4 and 3.2 mm ventral to the surface of the brain. We pooled data obtained with the two viruses, as each gave similar results. For retrograde labeling experiments, 500 nl of cholera toxin subunit B (CTB; catalog #C-34776 Life Technologies) was injected into the MEC at 3.6 mm lateral to the midline between the lambda suture and the underlying sinus, at 9° from vertical and at a depth of 1–3 mm.

Electrophysiological recordings. Three to 5 weeks after virus injection, horizontal brain slices were prepared, and whole-cell patch-clamp recordings were made from neurons in layers II–VI of the MEC, as described previously (Nolan et al., 2007). Slices were cut at $\sim 4^\circ\text{C}$ in solution with the following composition (in mM): NaCl 86, NaH_2PO_4 1.2, KCl 2.5, NaHCO_3 25, Glucose 25, Sucrose 50, CaCl_2 0.5, and MgCl_2 7. For maintenance and recording the extracellular solution had the following composition (in mM): NaCl 124, NaH_2PO_4 1.2, KCl 2.5, NaHCO_3 25, glucose 20, CaCl_2 2, and MgCl_2 1. The intracellular solution had the following composition (in mM): K gluconate 130; KCl 10, HEPES 10, MgCl_2 2, EGTA 0.1, Na_2ATP 2, Na_2GTP 0.3 Na phosphocreatine 10, biocytin 5.4. All recordings took place at $36 \pm 2^\circ\text{C}$.

ChR2 was activated by 470 nm light, with irradiance of $\sim 145 \text{ mW}/\text{mm}^2$, from an LED (Thorlabs) attached to the epifluorescence port of the microscope (BX-51; Olympus). Light stimuli had a duration of 10 ms and were repeated every 20 s for a minimum of five sweeps. Recordings used Multiclamp or Axoclamp amplifiers (Molecular Devices), and data were sampled at 20 kHz and digitized using a Digidata 1320A (Molecular

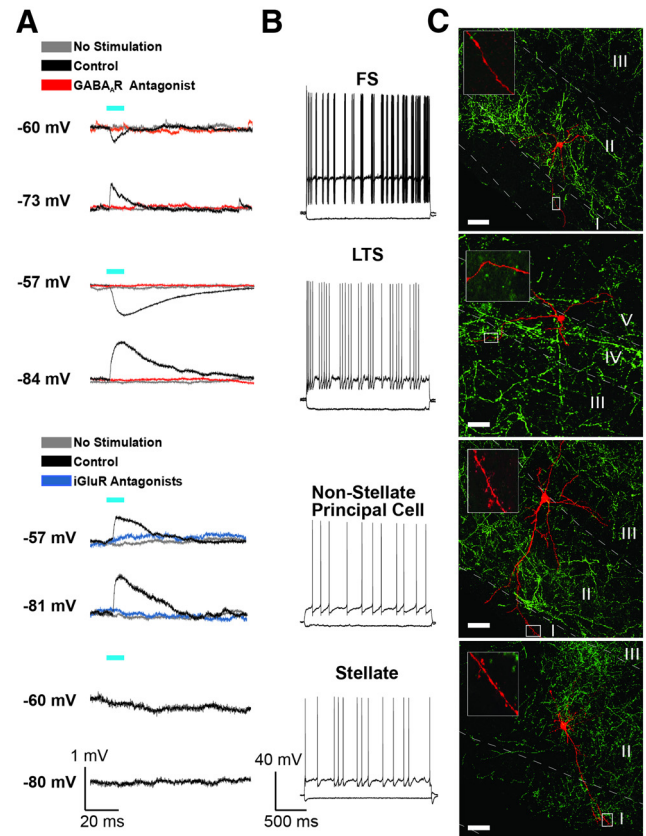


Figure 2. Responses to activation of MS fibers across different MEC cell types. **A**, Examples of averaged ($n = 5$) IPSPs and EPSPs evoked by photostimulation (blue bar) of ChR2-positive MS axons recorded at holding potentials on either side of the chloride reversal potential. No stimulation (gray), GABA_AR (red), and iGluR (blue) blockade traces are also shown. **B**, Representative responses of FS interneurons, LTS interneurons, NSPCs, and SCs to injection of positive and negative current steps. The cells are the same as in **A**. **C**, Streptavidin (red) staining of biocytin-filled cells recorded in **A** and **B**. ChR2-venus MS axons are in green. Inset displays $40\times$ image of dendritic regions indicated in the main image, showing the absence and presence of spines in inhibitory and excitatory neurons, respectively. Scale bar, 50 μm .

Devices). Series resistance was $\leq 30 \text{ M}\Omega$. Bridge balance and pipette capacitance neutralization were applied in current clamp, and series resistance compensation in voltage-clamp. An experimentally determined liquid junction potential of 12.7 mV was not corrected for. The reversal potential of IPSPs was estimated by fitting a polynomial function to plots of the mean IPSP amplitude as a function of baseline membrane potential (between -80 and -50 mV). Pharmacological agents were obtained from Abcam and were added to the standard extracellular solution at the following concentrations (in μM): NBQX 5 and D-APV 50 to block ionotropic glutamate receptors (iGluRs); picrotoxin 50 to block GABA_A receptors (GABA_AR); and atropine 1, mecamylamine 60, and methyllycaconitine 0.05 to block acetylcholine receptors (AChRs).

Cell identification. We used a hierarchical scheme to distinguish stellate cells (SCs), nonstellate principal cells (NSPCs), FS interneurons, and LTS interneurons. SCs were first identified by location in layer II, a sag response of < 0.7 (SCs, 0.58 ± 0.01 ; NSPCs, 0.86 ± 0.01 ; LTS interneurons, 0.87 ± 0.02 ; FS interneurons, 0.87 ± 0.16), and input resistance of $< 90 \text{ M}\Omega$ (SCs, $38.4 \pm 3.1 \text{ M}\Omega$; NSPCs, $222.9 \pm 10.6 \text{ M}\Omega$; LTS interneurons, $276.0 \pm 25.2 \text{ M}\Omega$; FS interneurons, $94.9 \pm 19.7 \text{ M}\Omega$; cf. Garden et al., 2008; Pastoll et al., 2013). Putative interneurons were next distinguished from NSPCs by an afterhyperpolarization (AHP) of $\geq 10 \text{ mV}$ (SCs, $5.8 \pm 0.5 \text{ mV}$; NSPCs, $0.6 \pm 0.4 \text{ mV}$; LTS interneurons, $13.3 \pm 0.6 \text{ mV}$; FS interneurons, $21.6 \pm 4.0 \text{ mV}$; Jones and Bühl, 1993; Sills et al., 2012; Couey et al., 2013). LTS interneurons were then identified by a rheobase of $\leq 120 \text{ pA}$ (SCs $315.1 \pm 32.1 \text{ pA}$; NSPCs, $107.1 \pm 5.1 \text{ pA}$; LTS interneurons, $72 \pm 6.5 \text{ pA}$; FS interneurons, $327.4 \pm 60.6 \text{ pA}$). The

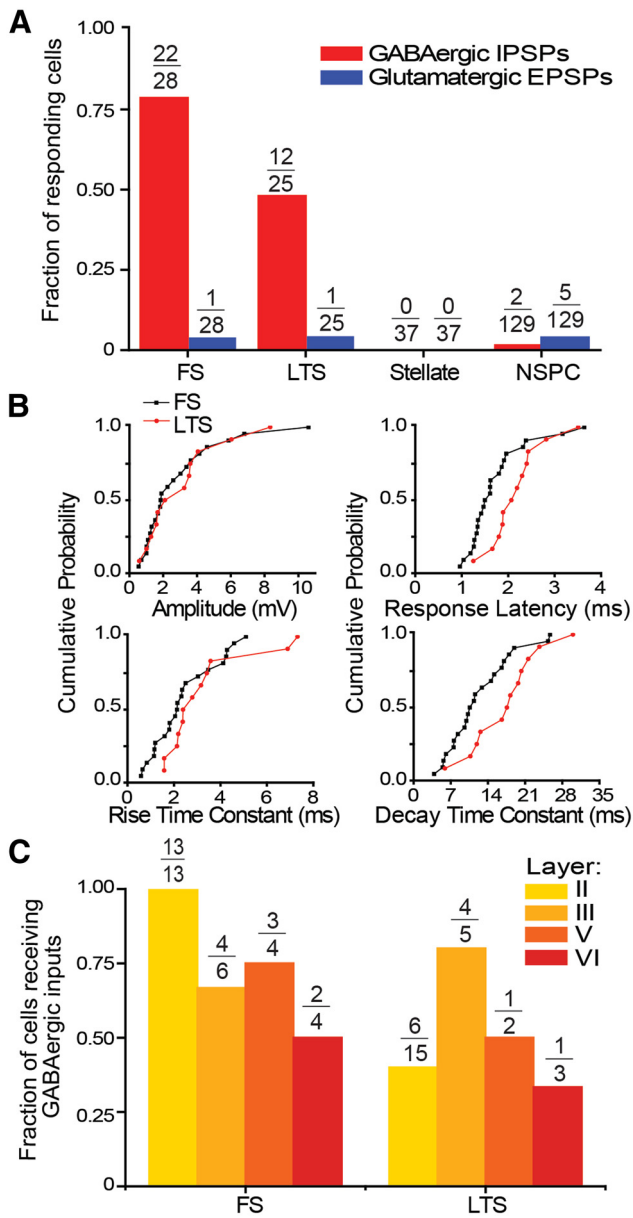


Figure 3. MS GABAergic fibers target FS and LTS interneurons in MEC. **A**, Fraction of neurons of each cell type responding to photostimulation in MEC. Numbers indicate responding cells and total number of recorded cells. **B**, Cumulative probability plots of IPSP amplitude, latency, rise, and decay time constants for responsive inhibitory neurons. **C**, Fraction of FS and LTS interneurons in each layer receiving GABAergic input from the MS.

remaining neurons were classified as FS interneurons. With these criteria neuronal firing properties during injection of current steps sufficient to trigger spiking for a duration of 3 s were similar to previous descriptions (e.g., median interspike interval: SCs, 108.0 ± 6.5 ms; NSPCs, 168.6 ± 8.89 ms; LTS interneurons, 61.7 ± 6.1 ms; FS interneurons, 19.7 ± 4.2 ms; $p < 1 \times 10^{-17}$, ANOVA; $p < 0.005$ for FS vs SC or NSPC, and LTS vs NSPC, Tukey's test; mean action potential half-width (in ms): SCs, 0.60 ± 0.02; NSPCs, 0.78 ± 0.02; LTS interneurons, 0.52 ± 0.03; FS interneurons, 0.29 ± 0.06 ms; $p < 1 \times 10^{-24}$, ANOVA; $p < 0.005$ for FS vs SC, NSPC, or LTS, and LTS vs NSPC, Tukey's test; cf. Jones and Bühl, 1993; Pastoll et al., 2013).

To further evaluate our electrophysiological classification of interneurons, we examined filled cells for the presence of dendritic spines, which are typically found in principal cells, but not interneurons (Canto et al., 2008). After recording, a subset of slices was placed in 4% paraformaldehyde (PFA) overnight, washed three times with 0.01 M PBS and blocked for 3 h with 0.01

M PBS containing 0.5% (w/v) Triton X-100 (PBT, 0.5%), 0.3% normal goat serum, and 0.2% bovine serum albumin. Slices were then incubated overnight at room temperature with streptavidin Alexa Fluor-555 or Alexa Fluor-488 [1:2000; Life Technologies (RRIDs: AB_2307336 and AB_23153831)] in 0.01 M PBS and PBT 0.5%, washed in PBS, and mounted with Mowiol solution. Dendritic spines were present in electrophysiologically identified SCs ($n = 2$ of 2) and NSPCs ($n = 4$ of 4), and were absent in FS interneurons ($n = 3$ of 3) and LTS interneurons ($n = 3$ of 3).

Immunohistochemistry. Animals were transcardially perfused with 4% PFA in PBS. Sections were prepared and processed for immunohistochemistry as described previously (Nolan et al., 2007) and with the following primary antibodies: goat anti-chAT (1:200; RRID:AB_2079751, Millipore) for labeling cholinergic neurons; mouse anti-parvalbumin (PV; 1:2000; RRID:AB_10000343, Swant) and anti-GAD 67 (1:200; RRID: AB_2278725, Millipore) for labeling GABAergic neurons; and NeuroTrace 640/660 fluorescent Nissl stain (1:2000; RRID:nlx_152414, Life Technologies). The following secondary antibodies were used: donkey anti-goat far red-647 (1:500; RRID:AB_141844, Invitrogen); goat anti-mouse Alexa Fluor-488 (1:800; RRID:AB_141367, Invitrogen). Imaging of labeled sections used a Nikon A1R confocal microscope with a 26.8 μm pinhole diameter and a 4.95 μm optical slice. MS mCherry or venus-positive cells coexpressing ChAT, GAD-67, or PV were identified on a single focal plane and visually inspected for double labeling.

Data analysis and statistics. Electrophysiological data were analyzed using Igorpro (WaveMetrics), Clampfit (Molecular Devices), and Spike2 (CED). Rise and decay time constants were calculated by fitting a double exponential function to synaptic response waveforms. Normality of groups was assessed with the Shapiro–Wilk test. Comparisons between groups with Gaussian distributed data used *t* test or ANOVA followed by Tukey's *post hoc* comparison. The Wilcoxon signed rank test, Kruskal–Wallis ANOVA, and Kolmogorov–Smirnov (KS) test were used for comparing nonparametric data. For quantification of fluorescence, the mean signal density in each layer was normalized to the peak signal density across all layers.

Results

To assess the identity of MS neurons projecting to the MEC, we injected the retrograde tracer CTB into the MEC ($n = 4$ mice). Within the MS, 41.7 ± 0.7% of cells labeled with CTB (72 of 168 cells) were positive for GAD67, the most common GAD isoform in the MS (Castañeda et al., 2005), and 6.6 ± 1.9% (13 of 204 cells) were positive for PV (data not shown), while 18.1 ± 3.7% of GAD67 (72 of 423 cells) and 6.9 ± 2.8% of PV cells (13 of 233 cells) were CTB positive. Thus, a large fraction of the projection from the MS to the MEC originates from GABAergic neurons, with a subset positive for PV. A further 13.2 ± 2.9% of CTB cells (26 of 204) were colabeled with ChAT, while 14.1% of ChAT cells (26 of 207 cells) were CTB positive, indicating that cholinergic neurons also project from the MS to the MEC.

To investigate the functional organization of this projection, we injected AAV expressing ChR2 conjugated with either mCherry or Venus into the MS (Fig. 1A). With our injection protocol, we found labeled cell bodies in 67.0 ± 5.2% of the area of the MS ($n = 4$ mice; Fig. 1B). Of neurons labeled with viral reporter, 55.0 ± 0.04% of cells (223 of 402 cells) were labeled with antibodies against GAD67, 9.5 ± 3.4% were positive for PV (24 of 284 cells), and a further 4.8 ± 1.4% were positive for ChAT (13 of 284 cells), while 61.0 ± 7.2% (223 of 357 cells), 33.1 ± 7.8% (24 of 71 cells), and 16.3 ± 6.0% (13 of 116 cells), respectively, of GAD67, PV, and ChAT cells were colabeled with viral reporter. Within the MEC, we observed a consistent laminar organization of labeled axons (Fig. 1C). We quantified this for horizontal MEC slices 2.6 mm from the dorsal surface of the brain. Here, fluorescence was significantly higher in layers II and V compared with layers I and VI ($p = 0.0002$, ANOVA; $p < 0.05$ for significant differences between layers, Tukey's test; Fig. 1C). A similar organization was seen in more dorsal and ventral slices (data not

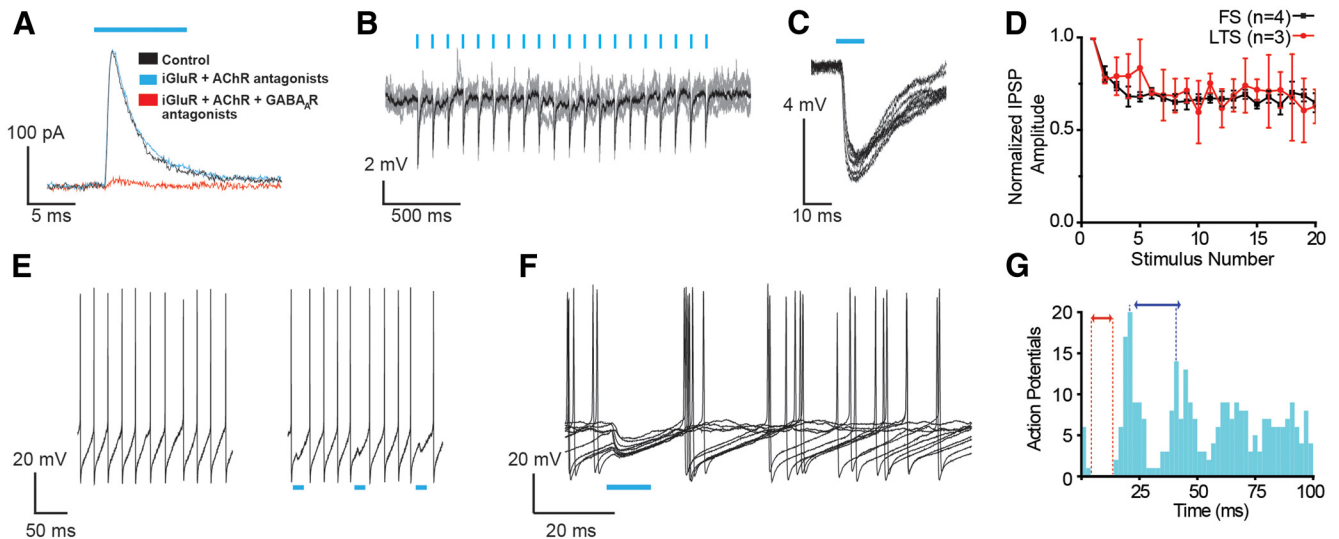


Figure 4. MS GABAergic fibers entrain FS and LTS interneuron firing. **A**, Voltage-clamp responses in control (black), in the presence of iGluR and AChR antagonists (blue); and in the presence of iGluR, AChR, and GABA_AR antagonists (red). Holding potential, 0 mV. **B**, Example responses of an FS interneuron to activation of MS GABAergic input at theta frequency (10 Hz). Mean trace, black; individual traces, gray. **C**, Ten consecutive responses from **B** on an expanded time scale. **D**, Normalized IPSP amplitude plotted as a function of stimulus number. **E**, Example response during the injection of current sufficient for maintained action potential firing without (left) and with (right) theta frequency activation of MS inputs to an FS neuron. **F**, Ten consecutive responses triggered from the time of each light stimulus illustrate entrainment of rebound spikes. **G**, Binned counts from 100 stimuli of action potentials as a function of time from the light pulse, illustrating measurement of pause time (red arrow) and frequency (blue arrow).

shown). Thus, our approach enables the expression of ChR2 by neurons in the MS and in their axonal projections to the MEC.

To evaluate synaptic responses of neurons in the MEC following expression of ChR2 in the MS, we made patch-clamp recordings from neurons in layers II, III, V, and VI ($n = 110, 46, 30,$ and 33 , respectively) and activated projecting axons with blue light. We observed fast EPSPs ($n = 7$; 10–90% rise time, 2.7 ± 1.0 ms) and fast IPSPs ($n = 36$; 10–90% rise time, 2.23 ± 0.21 ms; Fig. 2A). IPSPs reversed polarity at -68.6 ± 0.9 mV ($n = 24$) and were abolished by picrotoxin ($n = 16$ of 16, Fig. 2A; also see Fig. 4A), indicating that they are mediated by GABA_ARs. EPSPs did not reverse polarity and were abolished by perfusion of D-APV and NBQX ($n = 4$ of 4; Fig. 2A), indicating that they are glutamatergic.

We next evaluated the distribution and properties of responses among different cell types. Cells were initially classified as putative FS interneurons, LTS interneurons, SCs, or NSPCs ($n = 28, 25, 37,$ and 129 , respectively; see Materials and Methods; Fig. 2B,C). This classification scheme, which is based on measurements of the sag, input resistance, action potential AHP, and rheobase, correctly separates neurons with firing properties and morphology associated with each cell group (Jones and Bühl, 1993; Couey et al., 2013; Pastoll et al., 2013). Light stimulation evoked GABAergic IPSPs in a high proportion (78.6%) of FS and a smaller fraction of LTS neurons (48.0%; Fig. 3A). For FS and LTS neurons, the light-evoked IPSP amplitude (2.8 ± 0.5 and 3.1 ± 0.7 mV; $p = 0.93$, KS test; Fig. 3B) and rise time constant (2.4 ± 0.3 and 3.3 ± 0.6 ms; $p = 0.44$, KS test) were similar, whereas the response latency (1.7 ± 0.1 and 2.2 ± 0.2 ms; $p < 0.02$, KS test) and decay time constant (12.4 ± 1.3 and 17.4 ± 1.9 ms; $p < 0.02$, unpaired t test) were lower in FS neurons. At least half of FS interneurons in layers III–VI, and all FS interneurons in layer II, received GABAergic inputs (Fig. 3C). GABAergic responses were also present in LTS cells in all layers examined (Fig. 3C). Light stimulation evoked GABAergic responses in only 1.6% of NSPCs and in no SCs (Fig. 3A). We observed glutamatergic EPSPs in similar fractions of NSPCs and interneurons (<5%), but not in any SCs (Fig. 3A). GABAergic responses to MS input did not appear to be mediated by feed forward excitation of local interneu-

rons as their underlying synaptic currents were maintained during block of iGluRs and AChRs ($n = 6$; control, 251.8 ± 116.8 pA; blockers, 202.8 ± 70.7 pA), but were again abolished by picrotoxin (14.3 ± 7.2 pA; $p < 0.001$, Kruskal-Wallis ANOVA; Fig. 4A). Furthermore, the latency of GABAergic IPSPs was both short (Fig. 3C) and invariable (SD, 0.33 ± 0.12 ms; range, 0.13–0.94 ms; Fig. 4C). Together, these data indicate that the MS sends monosynaptic inhibitory projections primarily to interneurons in the MEC. Glutamatergic responses are detected less frequently and do not appear to distinguish between NSPCs and interneurons, while SCs do not appear to respond to glutamatergic or GABAergic input from the MS.

We next sought to establish whether theta frequency activation of GABAergic input from the MS can affect spike output from neurons in the MEC. We first asked whether synaptic responses accurately follow stimulation at 10 Hz. We found that IPSPs on FS and LTS neurons were maintained during 2 s of stimulation (Fig. 4B–D). To determine whether IPSPs could entrain firing by interneurons, we examined responses during injection of constant current with amplitude just sufficient to sustain action potential firing (Fig. 4E–G). We observed that light stimulation induced pauses in spike firing followed by periods of rhythmic spiking, with little effect on the overall spike rate (control, 43.2 ± 14.5 Hz; light stimulation, 47.7 ± 15.9 Hz; $p = 0.42$, paired t test). The duration of the pause in spiking was not significantly different FS and LTS interneurons (14.4 ± 2.5 and 21.7 ± 10.0 ms; $p = 0.17$, unpaired t test) and was relatively invariant (SD: FS interneurons, 4.3 ± 1.3 ms; LTS interneurons, 2.6 ± 1.1 ms; $p = 0.11$, unpaired t test), while the interval between the first and second spikes was typically in the low gamma band for LTS (25–43 Hz) and in the high gamma band (50–163 Hz) for FS interneurons (34.8 ± 5.3 and 118.2 ± 26.5 ms respectively; $p = 0.046$, unpaired t test), reflecting the intrinsic spike frequency of each cell type. These data demonstrate that MS GABAergic inputs to the MEC can follow 10 Hz stimulation and, in doing so, can entrain gamma frequency spike trains in MEC interneurons.

Discussion

We demonstrate that GABAergic projections from the MS synapse onto both FS and LTS interneurons in all layers of the MEC,

but rarely synapse onto excitatory cells. Projections from the MS generate inhibitory GABA_A receptor-mediated postsynaptic responses that are maintained during stimulation at theta frequency and can entrain activity of responding cells. We observed glutamatergic responses to MS activation much less frequently and in a similar proportion of responding interneurons and NSPCs. We did not observe glutamatergic or GABAergic responses in layer II SCs. The specificity of connectivity between the MS and MEC imposes constraints on mechanisms for generation of theta oscillations and spatial firing by neurons in the MEC.

Our finding of preferential targeting of inhibitory inputs to interneurons in the MEC is consistent with anatomical findings in the hippocampus (Freund and Antal, 1988). Thus, while the hippocampus and MEC differ in their laminar organization, principles for inhibitory control of each structure by the MS may be similar. It is important to consider the degree to which our analysis might underestimate connectivity through incomplete infection of all projection neurons in the MS. This is unlikely to explain the absence of inhibitory responses of NSPCs and SCs, as NSPCs and SCs are intermingled with interneurons, and inhibitory responses were observed in the majority of interneurons in all layers. Thus, our approach clearly activates inhibitory axons from the MS. Our finding that glutamatergic projections from MS to MEC are relatively rare is consistent with the lower percentage of glutamatergic projections from MS to the hippocampus (Colom et al., 2005; Henderson et al., 2010). However, while our injections likely infect glutamatergic neurons in the MS, as they are found adjacent to GABAergic neurons (Colom et al., 2005), our data nevertheless do not rule out the possibility that glutamatergic projections are more difficult to activate. Our finding that glutamatergic and GABAergic synaptic responses are absent in SCs is consistent with low levels of connectivity found with rabies virus tracing of inputs to SCs (Rowland et al., 2013).

What implications does the specificity of targeting of MS GABAergic projections to the MEC have for generation of theta rhythms in entorhinal–hippocampal circuits? A majority of interneurons across all layers of the MEC and subregions of the hippocampus have similar preferred firing phases with respect to the theta rhythm (Mizuseki et al., 2009). Because GABAergic fibers appear to specifically target interneurons in the hippocampus (Freund and Antal, 1988) as well as the MEC, GABAergic projections from the MS may coordinate theta firing by interneurons throughout the entorhinal–hippocampal circuit. Consistent with this idea, firing of GABAergic neurons in the MS is phase locked to hippocampal theta and on average precedes firing of hippocampal interneurons (Hangya et al., 2009). A possibility suggested by our results is that this GABAergic input from the MS entrains rebound firing of entorhinal interneurons rather than simply switching off their activity. Given recent evidence that SCs communicate exclusively via inhibitory interneurons (Couey et al., 2013; Pastoll et al., 2013), control of inhibitory networks by GABAergic projections from the MS may be well suited to contribute to roles of septal GABAergic neurons in spatial behaviors (Dwyer et al., 2007; Pang et al., 2011).

References

Brandon MP, Bogaard AR, Libby CP, Connerney MA, Gupta K, Hasselmo ME (2011) Reduction of theta rhythm dissociates grid cell spatial periodicity from directional tuning. *Science* 332:595–599. [CrossRef Medline](#)
 Canto CB, Wouterlood FG, Witter MP (2008) What does the anatomical organization of the entorhinal cortex tell us? *Neural Plast* 2008:381243. [CrossRef Medline](#)
 Castañeda MT, Garrido-Sanabria ER, Hernandez S, Ayala A, Reyna TA, Wu JY, Colom LV (2005) Glutamic acid decarboxylase isoforms are differ-

entially distributed in the septal region of the rat. *Neurosci Res* 52:107–119. [CrossRef Medline](#)
 Chrobak JJ, Buzsáki G (1998) Gamma oscillations in the entorhinal cortex of the freely behaving rat. *J Neurosci* 18:388–398. [Medline](#)
 Colgin LL, Denninger T, Fyhn M, Hafting T, Bonnevie T, Jensen O, Moser MB, Moser EI (2009) Frequency of gamma oscillations routes flow of information in the hippocampus. *Nature* 462:353–357. [CrossRef Medline](#)
 Colom LV, Castañeda MT, Reyna T, Hernandez S, Garrido-Sanabria E (2005) Characterization of medial septal glutamatergic neurons and their projection to the hippocampus. *Synapse* 58:151–164. [CrossRef Medline](#)
 Couey JJ, Witoelar A, Zhang SJ, Zheng K, Ye J, Dunn B, Czajkowski R, Moser MB, Moser EI, Roudi Y, Witter MP (2013) Recurrent inhibitory circuitry as a mechanism for grid formation. *Nat Neurosci* 16:318–324. [CrossRef Medline](#)
 Dwyer TA, Servatius RJ, Pang KC (2007) Noncholinergic lesions of the medial septum impair sequential learning of different spatial locations. *J Neurosci* 27:299–303. [CrossRef Medline](#)
 Freund TF, Antal M (1988) GABA-containing neurons in the septum control inhibitory interneurons in the hippocampus. *Nature* 336:170–173. [Medline](#)
 Garden DL, Dodson PD, O'Donnell C, White MD, Nolan MF (2008) Tuning of synaptic integration in the medial entorhinal cortex to the organization of grid cell firing fields. *Neuron* 60:875–889. [CrossRef Medline](#)
 Hafting T, Fyhn M, Bonnevie T, Moser MB, Moser EI (2008) Hippocampus-independent phase precession in entorhinal grid cells. *Nature* 453:1248–1252. [CrossRef Medline](#)
 Hangya B, Borhegyi Z, Szilágyi N, Freund TF, Varga V (2009) GABAergic neurons of the medial septum lead the hippocampal network during theta activity. *J Neurosci* 29:8094–8102. [CrossRef Medline](#)
 Henderson Z, Lu CB, Janzso G, Matto N, McKinley CE, Yanagawa Y, Halasy K (2010) Distribution and role of Kv3.1b in neurons in the medial septum diagonal band complex. *Neuroscience* 166:952–969. [CrossRef Medline](#)
 Jones RS, Bühl EH (1993) Basket-like interneurons in layer II of the entorhinal cortex exhibit a powerful NMDA-mediated synaptic excitation. *Neurosci Lett* 149:35–39. [CrossRef Medline](#)
 Koenig J, Linder AN, Leutgeb JK, Leutgeb S (2011) The spatial periodicity of grid cells is not sustained during reduced theta oscillations. *Science* 332:592–595. [CrossRef Medline](#)
 Meibach RC, Siegel A (1977) Efferent connections of the septal area in the rat: an analysis utilizing retrograde and anterograde transport methods. *Brain Res* 119:1–20. [CrossRef Medline](#)
 Mitchell SJ, Ranck JB Jr (1980) Generation of theta rhythm in medial entorhinal cortex of freely moving rats. *Brain Res* 189:49–66. [CrossRef Medline](#)
 Mitchell SJ, Rawlins JN, Steward O, Olton DS (1982) Medial septal area lesions disrupt theta rhythm and cholinergic staining in medial entorhinal cortex and produce impaired radial arm maze behavior in rats. *J Neurosci* 2:292–302. [Medline](#)
 Mizuseki K, Sirota A, Pastalkova E, Buzsáki G (2009) Theta oscillations provide temporal windows for local circuit computation in the entorhinal–hippocampal loop. *Neuron* 64:267–280. [CrossRef Medline](#)
 Newman EL, Gillet SN, Climer JR, Hasselmo ME (2013) Cholinergic blockade reduces theta-gamma phase amplitude coupling and speed modulation of theta frequency consistent with behavioral effects on encoding. *J Neurosci* 33:19635–19646. [CrossRef Medline](#)
 Nolan MF, Dudman JT, Dodson PD, Santoro B (2007) HCN1 channels control resting and active integrative properties of stellate cells from layer II of the entorhinal cortex. *J Neurosci* 27:12440–12451. [CrossRef Medline](#)
 Pang KC, Jiao X, Sinha S, Beck KD, Servatius RJ (2011) Damage of GABAergic neurons in the medial septum impairs spatial working memory and extinction of active avoidance: effects on proactive interference. *Hippocampus* 21:835–846. [CrossRef Medline](#)
 Pastoll H, Solanka L, van Rossum MC, Nolan MF (2013) Feedback inhibition enables theta-nested gamma oscillations and grid firing fields. *Neuron* 77:141–154. [CrossRef Medline](#)
 Quilichini P, Sirota A, Buzsáki G (2010) Intrinsic circuit organization and theta-gamma oscillation dynamics in the entorhinal cortex of the rat. *J Neurosci* 30:11128–11142. [CrossRef Medline](#)
 Rowland DC, Weible AP, Wickersham IR, Wu H, Mayford M, Witter MP, Kentros CG (2013) Transgenically targeted rabies virus demonstrates a major monosynaptic projection from hippocampal area CA2 to medial entorhinal layer II neurons. *J Neurosci* 33:14889–14898. [CrossRef Medline](#)
 Sills JB, Connors BW, Burwell RD (2012) Electrophysiological and morphological properties of neurons in layer 5 of the rat postsubiculum. *Hippocampus* 22:1912–1922. [CrossRef Medline](#)